A98-32418

AIAA-98-2517

LOW-FREQUENCY FLOWFIELD UNSTEADINESS DURING AIRFOIL STALL AND THE INFLUENCE OF STALL TYPE

Andy P. Broeren* and Michael B. Bragg†

University of Illinois at Urbana-Champaign
Urbana, Illinois 61801

Abstract

The flow past stalled airfoils is generally unsteady and can result in large force fluctuations. This paper addresses the relationship between airfoil stall type and the level of large-scale unsteady flow at stall. A total of 12 airfoils, encompassing different stalling characteristics were tested over a large angle of attack range at a Reynolds number of 300,000. Time-dependent lift data, wake hot-film data and flow visualization data were acquired. The time-dependent lift data were low-pass filtered with a 20 Hz cut-off to remove unwanted contributions to the fluctuating lift ($C_{l,rms}$) from model and lift-balance resonances. The results show that airfoils having trailing-edge stall experience minimal lift fluctuations at stall ($C_{l,rms} < 0.04$). The fluctuating lift for leading-edge stall airfoils increases sharply (to $C_{l,rms} \approx 0.04$) with the abrupt loss of lift associated with this stall type. For thin-airfoil stall types, the fluctuating lift gradually increases to high levels ($0.04 < C_{l,rms} < 0.08$) as maximum lift is attained. Finally, for airfoils having a combination of thin-airfoil and trailing-edge stall the lift fluctuations at maximum mean lift were very high ($C_{l,rms} > 0.08$). The fluctuating lift spectra for the latter two stall types contained distinct low-frequency peaks, indicating the large-scale unsteadiness associated with these stall types.

Introduction

The flow past airfoils inclined at stalling angles of attack can be dominated by large-scale unsteady flow, which develops over the airfoil despite steady free-stream and surface-boundary conditions. This flowfield unsteadiness can cause large force changes on airfoil models, wings, rotor blades and the like. Indeed, as early as the 1930's, B. Melvill Jones[1] observed "violent fluctuations" of lift and drag on airfoil models near stalling conditions. Mabey[2] suggests that low-frequency force changes on airfoils are a likely cause of wing buffet. Zaman, McKinzie and Rumsey[3] reported a low-frequency, quasi-periodic oscillation of the flow over an airfoil near stall and argue that the frequency and large lift oscillations may be responsible for instigating stall flutter of wings and blades. A better understanding of the unsteady flows past stalled airfoils is therefore required to avoid potential damage to aircraft or machinery and improve safety.

Airfoil stall can be classified into three basic types based upon the time-averaged characteristics of the flowfield. Following the work of Jones,[1] McCullough and Gault[4] conducted more detailed stall testing and established the presently accepted definitions of airfoil stall type. *Trailing-edge stall* is preceded by movement of the turbulent boundary-layer separation point forward from the trailing edge with increasing angle of attack. *Leading-edge stall* has abrupt flow separation near the leading edge generally without subsequent reattachment. The "abrupt" separation usually results from a small laminar separation bubble which "bursts" at stall and usually causes a sharp decrease in lift. *Thin-airfoil stall* is preceded by flow separation at the leading edge with reattachment (laminar separation bubble) at a point which moves progressively downstream with increasing angle of attack. Airfoil stall type is a function of several variables such as Reynolds number, surface roughness or free-stream turbulence. Therefore, any particular airfoil may exhibit a combination of stall types, or its stall type may change when flow conditions are changed.

---

* Graduate Research Assistant, Department of Mechanical and Industrial Engineering, Member AIAA
† Professor, Department of Aeronautical and Astronautical Engineering, Associate Fellow AIAA

Airfoil stall is a complex fluid flow problem involving separated flow, and some level of unsteadiness is expected. There is evidence in the literature that some stall types exhibit more intense unsteadiness than others, but there are conflicting conclusions. For example, Jones[1] reported that the "violent fluctuations" of lift and drag occurred for trailing-edge and thin-airfoil stall airfoils, but not for leading-edge stall airfoils. On the other hand, McCullough and Gault[4] state that an NACA 63_1-012 airfoil, which has a leading-edge stall type, experienced "violent buffeting" at angles of attack just beyond the maximum lift coefficient ($C_{l,max}$). Also, Gault[5] observed unsteady flow past a leading-edge stall NACA 63-009 at $C_{l,max}$. There is some agreement for thin-airfoil stall type, as McCullough and Gault[6] reported low-frequency flow unsteadiness for an NACA 64A006 airfoil at angles of attack near stall. This airfoil has a thin-airfoil stall type, and these observations are consistent with Jones.[1] Mabey[2] reviews some existing data in an attempt to predict the level of root-mean-square normal force fluctuations at stall, but he does not address airfoil stall type. These studies did not contain detailed data about the frequency content of the unsteady flows, which is important in connecting the force changes to buffet or stall flutter.

As mentioned above, Zaman et al.[3] conducted a detailed study of unsteady flow past an LRN(1)-1007 airfoil near stall and reported Strouhal numbers of 0.02 for the flow oscillation at angles of attack near stall. Here, the Strouhal number is defined as: $St = fc\sin\alpha / U_\infty$, where f is the dimensional frequency, c is the chord and U_∞ is the free-stream speed. The value of $St = 0.02$ is considered very low as it is an order of magnitude lower than that of bluff-body shedding, which typically has frequencies of $St = 0.2$. For this reason, this behavior has simply been called the "the low-frequency flow oscillation" to distinguish it from bluff-body shedding. The data indicated that the unsteady oscillation was very intense and involved a periodic switching of the airfoil flowfield between stalled and unstalled conditions. The corresponding force fluctuations were very large, up to 50% of the mean lift coefficient. The authors classified the LRN(1)-1007 airfoil as having a combination of thin-airfoil and trailing-edge stall types.

Research into this low-frequency oscillation on the LRN(1)-1007 airfoil was subsequently performed by others[7-10] and the features of unsteady flowfield are well known. For example, Bragg et al.[9] present flow visualization data which clearly shows the laminar separation bubble near the leading edge increase in chordwise extent (characteristic of thin-airfoil stall) and turbulent boundary-layer separation (characteristic of trailing-edge stall) as the angle of attack is increased to maximum lift. Broeren[11] performed two-component laser-Doppler velocimeter measurements for the unsteady flowfield on the LRN(1)-1007. These results showed an interaction between the separation bubble reattachment and the turbulent boundary-layer separation as the airfoil stalls and unstalls. Thus, there may be a relationship between the airfoil stalling characteristics and the low-frequency oscillation. Further, various reports show little fundamental change in the character of the low-frequency oscillation over a Reynolds number range from 75,000 to 1,400,000.[7,9] Very similar low-frequency unsteady stall behavior has been documented for a variety of Reynolds numbers in other studies[2, 12-14] and the reported frequencies convert to Strouhal numbers less than or approximately equal to 0.02.

In an effort to better understand what factors contribute to unsteady flow near stall, this study focuses on relating the level of flowfield unsteadiness to airfoil stall type. The purpose of this paper is to resolve the apparent disagreement over which airfoil stall types contain large-scale unsteady flow near stall and determine if there is a relationship between stall type and the low-frequency flow oscillation as suggested above. To accomplish these objectives, time-dependent lift measurements, wake hot-film velocity measurements and flow visualization were carried out for a total of 12 different airfoils, encompassing different stalling characteristics. The two-dimensional airfoil models were tested over an angle of attack range from 0° to 25° and at a chord Reynolds number (Re) of 300,000. The level of unsteadiness was determined from the root-mean-square of the fluctuating lift coefficient ($C_{l,rms}$) and the frequency content was determined from spectral analysis of the lift and wake hot-film data. The lift curves and surface-oil-flow visualization data were used to determine the stall type of each airfoil tested. For the airfoils tested here, the results showed that thin-airfoil and combination thin-airfoil and trailing-edge stall types had the most intense low-frequency lift fluctuations, occurring very close to $C_{l,max}$. The trailing-edge and leading-edge stall types did not exhibit large fluctuations until after the angle of attack had been increased above maximum lift. These results are discussed in concert with previously published results.

Experimental Method and Apparatus

Wind-Tunnel Facility and Ancillary Equipment

All measurements were carried out in the Subsonic Aerodynamics Laboratory at the University

of Illinois, utilizing the low-speed, low-turbulence wind tunnel. The wind tunnel is a conventional indraft open-return type which has a four inch thick honeycomb flow straightener followed by four anti-turbulence screens. The turbulence levels in the empty 3 foot by 4 foot test section are less than 0.1% at all operating speeds.

The general experimental apparatus is shown in Fig. 1. The airfoil models (12-inch chord by 33.625-inch span) were mounted horizontally between 3/8-inch thick Plexiglas splitter plates to isolate the ends of the model from the tunnel side-wall boundary layers and the support hardware. The gap between each end of the models and the splitter plates was nominally 0.05 inches. One end of the airfoil model (far side of Fig. 1) was actuated to adjust and measure the angle of attack. The angle of attack was measured using a Bourns model 6574 precision rotary potentiometer. As shown in Fig. 2, the opposite end of the model is connected to the lift carriage which contains linear ball bearings and spherical bearings to minimize frictional effects in vertical translation on a precision ground shaft. The lift force was measured directly via a connecting rod from the lift carriage to an Interface Inc. SM-25 strain gauge load cell. A compression spring was used to support the weight of the lift carriage and model. For the present experiments, the load cell was routinely calibrated in its measurement position to determine the effects of mechanical hysteresis and/or other nonlinearities. The free-stream dynamic pressure was measured upstream of the model between the splitter plates with a single pitot-static probe.

The frequency content of the flow past the airfoils was measured in the wake. A TSI 1210-20 hot-film probe was mounted in a single location on a rigid strut at 0.47 chords downstream and 0.20 chords above the airfoil trailing edge at $\alpha = 0°$ (see Fig. 2). This probe location corresponded to previous wake frequency measurements and the phase-averaged LDV data of Broeren and Bragg.[10] The hot-film sensor was not calibrated to compute velocity as only the voltage was required to provide frequency information.

A total of 12 airfoil sections were tested in this study and are shown in Fig. 3. The airfoils were selected based upon their expected stall type. References 15-17 provide the coordinates, more performance data (including drag) and contour accuracy data for these models.

Data Acquisition

All of the ambient conditions and wind-tunnel data were acquired using an IBM-compatible microcomputer equipped with an analog-to-digital

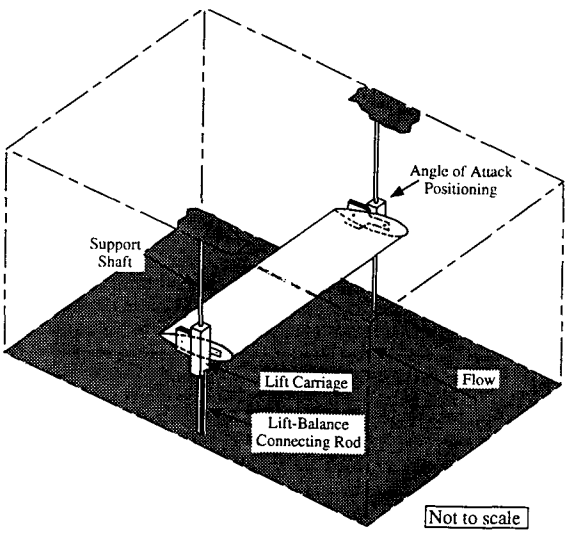

Fig. 1 General experimental apparatus (splitter plates not shown for clarity).

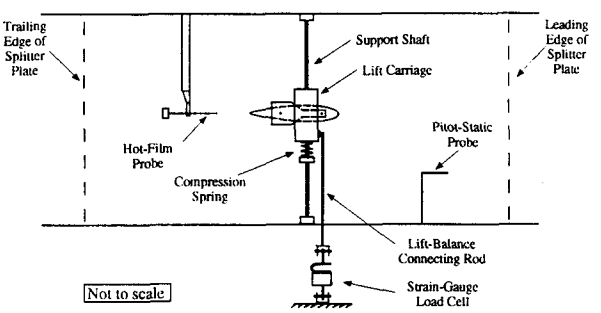

Fig. 2 Side-view of the test-section apparatus.

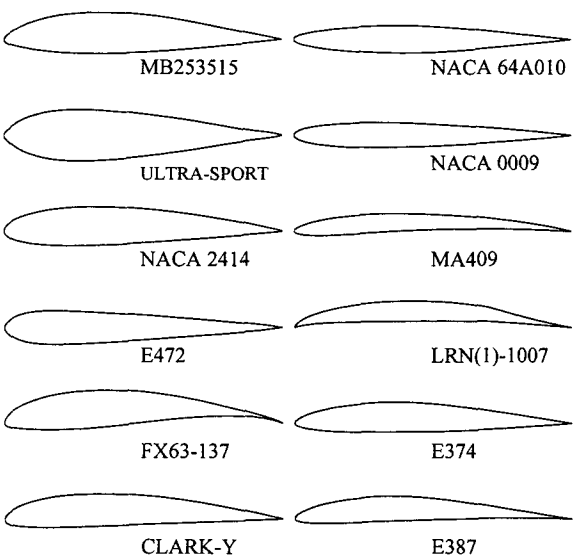

Fig. 3 The airfoils tested.

(A/D) conversion board. All data were acquired at Re = 300,000 and for α = 0° to 25°. The lift and hot-film signals were sampled for 5 seconds at a rate of 1,000 samples/sec (5,000 samples) and all of the time-dependent voltages were written to disk. The lift and hot-film signals were (analog) low-pass filtered with a 500 Hz cut-off. Detailed data were acquired for airfoils exhibiting unsteady stalling characteristics. Power spectra of both the lift and hot-film signals were acquired where appropriate using a Wavetek model 5830A Digital Signal Analyzer which interfaced with the data acquisition computer via GPIB.

Flow Visualization

Surface-oil-flow visualization was also performed for each of the airfoils tested. A light coat of oil containing fluorescent dye was sprayed on the surface of the model. The oil was allowed to flow for 20 to 30 minutes with the tunnel on. The resulting flow patterns in the oil gave information regarding time-averaged boundary-layer separation, reattachment and transition. These features were recorded for each airfoil as the angle of attack was increased into stall. The boundary-layer features can generally be determined to within ±2% chord.

Data Reduction and Uncertainty

The time-dependent lift voltages were digitally filtered and the lift coefficient (C_l) was calculated and corrected for wind-tunnel interference effects. Details on the digital filtering process are discussed below. The wind-tunnel correction procedures were carried out using methods similar to those given by Selig et al.[15] and Giguère and Selig.[18] The root-mean-square of the fluctuating lift coefficient ($C_{l,rms}$) was also computed from the time series data.

Strouhal numbers were calculated from the power spectra of the both the lift and hot-film signals. The peak frequency of each power spectrum was determined as the midpoint of the -3 dB bandwidth. This frequency and tunnel conditions were then used to calculate the Strouhal number. The uncertainty in the peak frequency was estimated to be plus or minus one half of the -3 dB bandwidth. Therefore, the uncertainty in the Strouhal number is higher for broader low-frequency peaks. The typical relative uncertainty in the Strouhal number was ±3%.

The experimental uncertainty was computed for the reduced quantities following the method presented in Coleman and Steele.[19] These calculations were included in the data reduction routines so that the variation in the uncertainty with angle of attack could be easily ascertained. The calculated uncertainties only include bias errors based upon 20:1 odds. The uncertainty in the angle of attack was ±0.15°. The relative uncertainty in the freestream velocity was ±0.90% at 50 ft/sec. The uncertainty in the mean lift coefficient is shown in Fig. 4, along with data from other facilities. The error bars are ±2 to 3% of the mean C_l. Agreement amongst the data is very good within the linear range and diverges after stall which may be due to large-scale unsteadiness which occurs for the E387 airfoil.

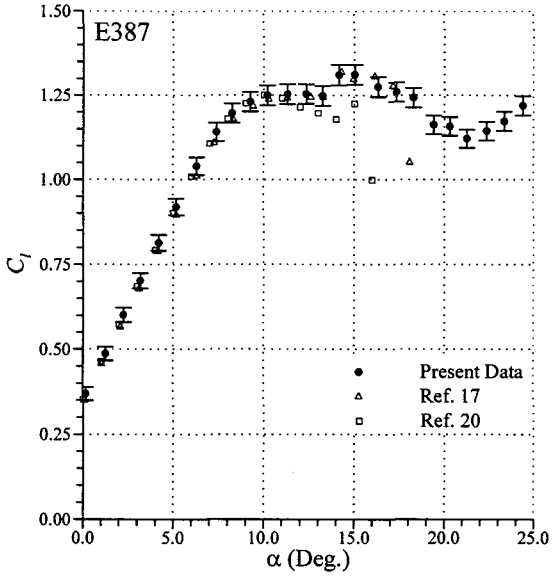

Fig. 4 Comparison of present data with data from other facilities for the E387 airfoil.

Lift-Balance Frequency Response

The lift balance used in this study was designed for unsteady lift measurements where the frequency response was a primary concern. Fortunately, the flow frequencies investigated were very small, less than 10 Hz. Several attempts were made to model and quantify the dynamics of the lift-balance mechanism and some of these results are documented here.

A simple second order system model of the lift balance was used to estimate the natural frequency of the system as well as the magnitude and phase response. Since the strain-gauge load cell deflected linearly over its operating range it was modeled as a spring with a constant of 2100 lbf/in. The small compression spring was of negligible stiffness relative to the load cell. The mass of the system was 3.2 lbm. The resulting natural frequency was approximately 80 Hz. A second order system model suggests that there should be no magnitude attenuation and no phase

difference for frequencies much less than the natural frequency, depending on the amount of damping within the system.

The characteristics of the airfoil models also played a role in the overall system dynamics. As shown in Fig. 3, the airfoils vary in thickness and there was a large variation in the structural compositions. The result of these two effects was a large range in the natural bending and torsional frequencies. These frequencies were estimated for some of the models assuming that the models were simply supported beams. The fundamental bending resonance was high, on the order of 100 Hz for the LRN(1)-1007 model. However, the fundamental torsional resonance was much lower, about 45 Hz. These are crude estimates, given the complexity of the geometry and composite composition, however, agreement with experiment is fairly good, as shown below.

Detailed investigations were conducted to evaluate the estimates of the natural frequencies given above. An accelerometer was used to analyze vibrations with the flow on. The spectra shown in Fig. 5 compare the frequency content of the wake hot-film, lift-balance and accelerometer (located on the model lower surface at the near end in Fig. 2) signals. The airfoil in Fig. 5 is the previously studied LRN(1)-1007 and the low-frequency peaks (at ≈ 4 Hz and ≈ 8Hz) in the hot-film spectra correspond to the fundamental and first harmonic of the low-frequency oscillation. The lift-balance spectrum also contains these peaks, and in addition, the broad peaks centered at approximately 38 Hz and 85 Hz. These frequency peaks correspond to the fundamental torsional resonance of the model and the lift-balance resonance, respectively. This is supported by other evidence as well. For example, when the freestream velocity was reduced by a factor of two, the low-frequency oscillation peaks occurred at a lower frequency, consistent with previous data.[3,7] However, the 38 and 85 Hz peaks remained at these frequencies which further suggests they are structural in origin. The lift spectra of other airfoils exhibiting low-frequency oscillations also contained a similar 85 Hz peak. The 38 Hz peak was not the same, but usually it occurred between 30 and 50 Hz. This further supports the conclusion that the 85 Hz peak is related to the lift balance and the 38 Hz peak is related to the model structure. In another test, a slight tapping on the surface of the airfoil model produced a frequency of about 40 Hz from the accelerometer. This again would indicate that the estimated torsional resonance of 45 Hz is fairly accurate.

It was also important to determine the magnitude and phase response of the system at the low frequencies. A rig was designed to drive the model at a known input frequency. The lift-balance signal (the output) and the input signal were measured simultaneously for comparison in the time domain. This procedure was repeated for several frequencies. The results showed no magnitude attenuation or phase difference up to a frequency of 3.5 Hz. Unfortunately, this procedure could not be carried out at higher frequencies due to equipment limitations.

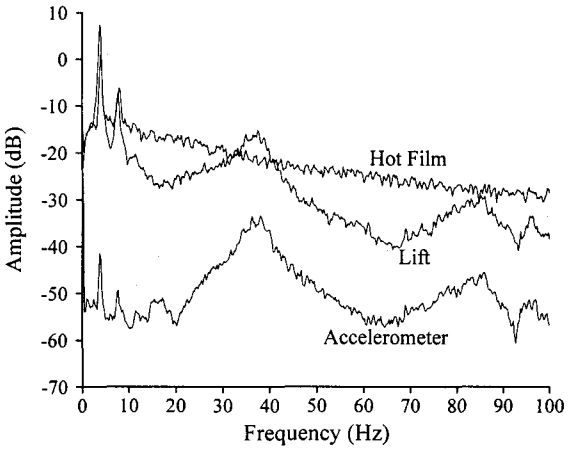

Fig. 5 Comparison of spectra from wake hot-film, lift-balance and accelerometer signals for the LRN(1)-1007 airfoil at α = 15°.

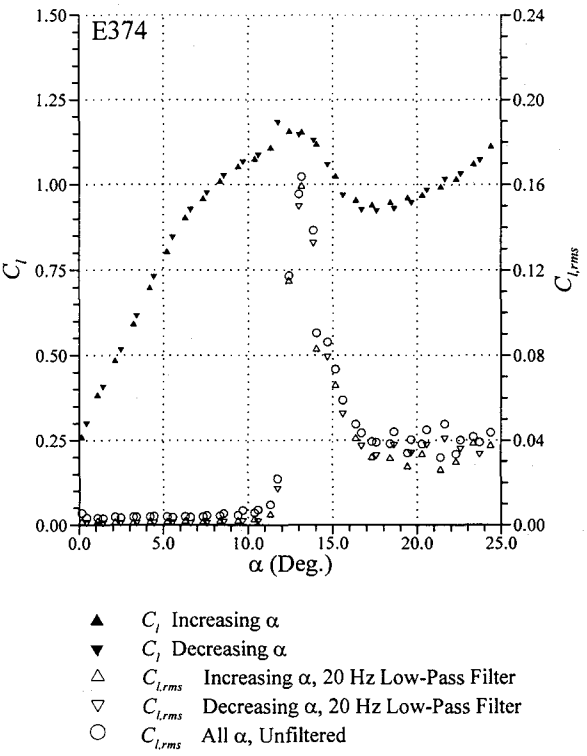

Fig. 6 Effect of filtering lift data for the E374 airfoil.

Table 1. Summary of Tme-Dependent Lift Measurements

Stall Type	Airfoil	Thickness	Camber	$C_{l,rms}$ at $C_{l,max}$
Trailing-edge	MB253515	15.0%	2.43%	0.005
	Ultra-Sport	18.6%	0.00%	0.005
Leading-edge	NACA 2414	14.0%	2.00%	0.010
	E472	12.1%	0.00%	0.005
Trailing-edge/Leading-edge	FX63-137	13.7%	5.94%	0.010
	CLARK-Y	12.0%	3.55%	0.005
Thin-airfoil	NACA 64A010	10.0%	0.00%	0.060
	NACA 0009	9.0%	0.00%	0.060
	MA409	6.7%	3.33%	0.080
Thin-airfoil/Trailing-edge	LRN(1)-1007	7.3%	5.90%	0.180
	E374	10.9%	2.24%	0.160
	E387	9.1%	3.90%	0.120

The 80 Hz frequency was also present in the lift-balance data, suggesting it is structural in origin (the lift balance) and not flow related. Based upon this and the validity of the second order system model, the time-dependent lift data should suffer negligible magnitude attenuation or phase discrepancy for frequencies less than 10 Hz.

The lift signal was digitally low-pass filtered with a 20 Hz cut-off to remove the unwanted contribution of model and lift-balance natural frequencies. The 8th order Butterworth filter was designed using MATLAB and implemented using a zero-phase delay, forward-reverse filtering algorithm. This means that the data were actually filtered twice (in opposite directions in time) to ensure that there was no phase delay, which resulted in a 16th order filter. Filtering the data had the effect of lowering the $C_{l,rms}$, however, this effect was relatively small, as shown in Fig. 6. The figure illustrates that most of the energy of the lift fluctuations was contained within the low frequencies. Low-pass filtering the $C_{l,rms}$ data with a 20 Hz cut-off eliminated the model and lift-balance resonances and ensured that the data from each airfoil are very comparable.

Results

Time-Dependent Lift Data

A summary of the time-dependent lift data is shown in Table 1, which classifies the airfoils tested by stall type. The stall type was determined from interpretation of the lift curves and flow visualization data. These data show that the airfoils having thin-airfoil stall and a combination of thin-airfoil and trailing-edge stall have the highest $C_{l,rms}$ levels at maximum lift, indicating large-scale unsteady flow. Of these, the $C_{l,rms}$ values for the combination stall type are nearly twice that for the pure thin-airfoil stall cases. The variation of $C_{l,rms}$ with angle of attack is presented below for representative airfoils in each category and the frequency content of the fluctuating lift is addressed in the following section.

The mean and fluctuating lift coefficients (C_l and $C_{l,rms}$) for the Ultra-Sport airfoil are shown in Fig. 7a as a function of angle of attack. The variation in C_l at stall was typical for the trailing-edge stall type. The plot shows how the $C_{l,rms}$ gradually increased as α increased beyond maximum lift. The relatively high levels of $C_{l,rms}$ (≈ 0.04) occurred for very high angles of attack ($\alpha > 18°$) and can be attributed to broad-band unsteadiness (from 0 to 20 Hz), with bluff-body shedding beginning at $\alpha = 22°$.

This behavior contrasted with the E472 which had a leading-edge stall type. The lift data, Fig. 7b, show the abrupt loss of lift at stall which is a trademark of the leading-edge stall type. The $C_{l,rms}$ level also changed abruptly with the loss of lift, increasing from less than 0.01 to almost 0.04. It is also interesting to note that the $C_{l,rms}$ remained high until the lift was recovered as the angle of attack was decreased beyond stall. This hysteresis in the mean lift is fairly well known[21] and the present data suggest that the fluctuating lift exhibits similar behavior.

Data for the combination trailing-edge and leading-edge stall type are shown in Fig. 7c, for the classic CLARK-Y airfoil. This combination stall type was determined from interpretation of the lift and flow visualization data. The mean and fluctuating lift trends contained elements of each stall type. The mean lift gradually decreased beyond stall (characteristic of

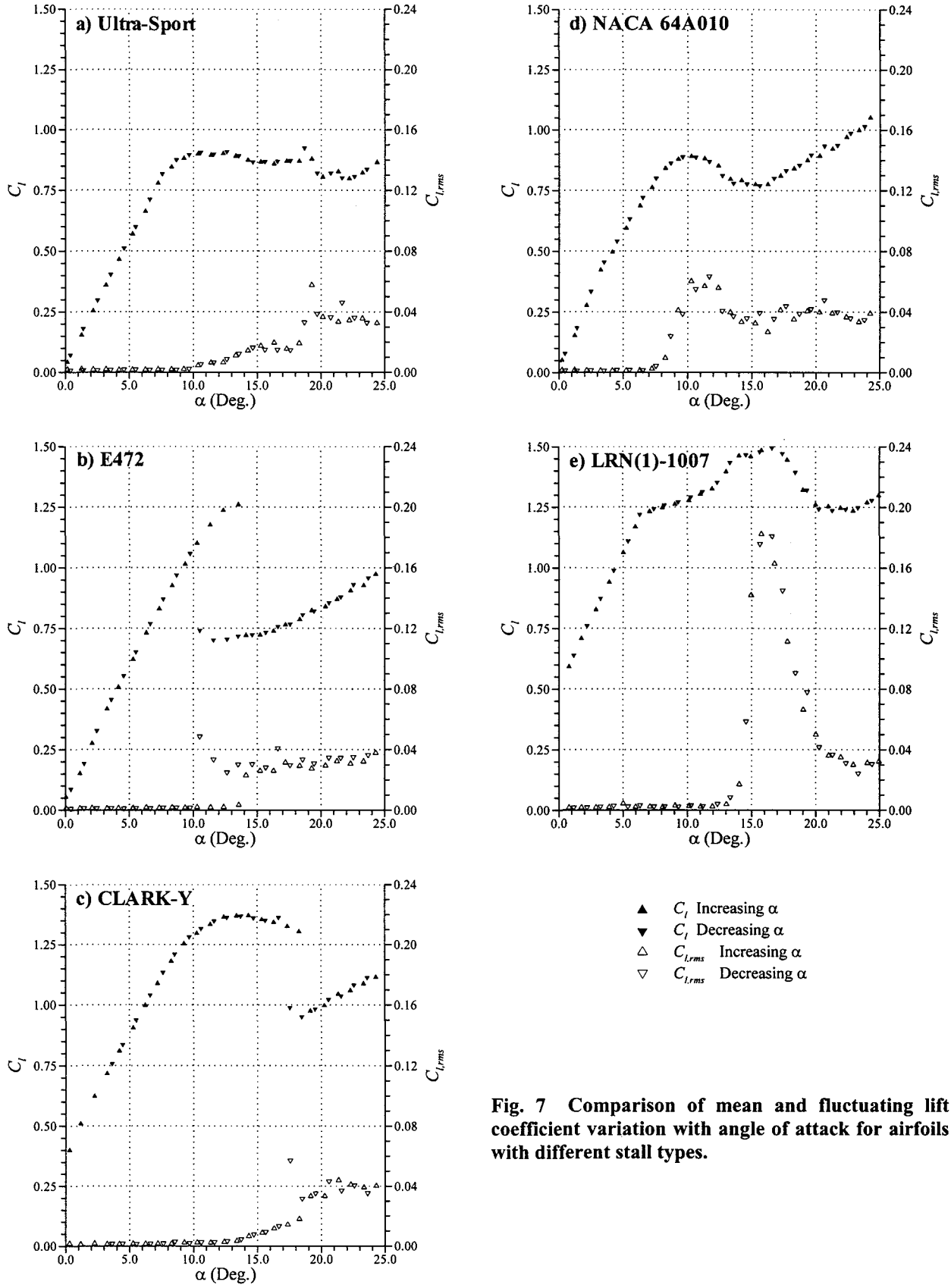

Fig. 7 Comparison of mean and fluctuating lift coefficient variation with angle of attack for airfoils with different stall types.

trailing-edge stall) until $\alpha = 19°$, where an abrupt drop occurred (characteristic of leading-edge stall). The fluctuating lift gradually increased to this point as well, then increased sharply and there was some hysteresis.

The lift data for the NACA 64A010 shown in Fig. 7d illustrates typical trends for airfoils having the thin-airfoil stall type. There was a distinctive change in slope associated with the formation of a separation bubble at $\alpha = 4°$ in Fig. 7d and a gentle stall, followed by gradual lift recovery with increasing incidence. The $C_{l,rms}$ variation was quite different from the previous cases. The $C_{l,rms}$ increased substantially (to 0.06) as maximum lift was attained, then decreased to the usual value of 0.04. These same trends in both mean and fluctuating lift were also observed in the NACA 0009 and MA409 airfoil data. The frequency spectra of the highest $C_{l,rms}$ values contained distinct low-frequency peaks.

The highest levels of unsteadiness were observed for airfoils with combination thin-airfoil and trailing-edge stall types. Data for these airfoils are shown in Fig. 7e for the representative LRN(1)-1007 airfoil (henceforward, "LRN"). The $C_{l,rms}$ peaks for these airfoils were extremely high and occurred almost exactly at the value of maximum lift, as shown for the LRN. However, the peaks in each case quickly drop off and the $C_{l,rms}$ values were about 0.04 for deep stall, which was similar to the other cases discussed above. These features are also shown in Fig. 6 for the E374 airfoil. As mentioned in the Introduction, the unsteady flow which accompanies the stall of the LRN has been well documented and it is obvious that the high values of the fluctuating lift coefficient resulted from the unsteady flow.

Frequency Content of the Fluctuating Lift

A key objective of this study was to identify large-scale, or low-frequency, oscillations associated with the unsteady flowfield of stalled airfoils. The spectra of the fluctuating lift for the trailing-edge, leading-edge and combination trailing-edge/leading edge stall types were distributed evenly over the low-frequencies (< 20 Hz). At higher frequencies there were some amplitude peaks associated with the model and balance natural frequencies as discussed above. Also for high angles of attack (> 20°) there were peaks at the bluff-body shedding frequencies which were discernible in both the lift and hot-film spectra.

The airfoils exhibiting distinct low-frequency unsteadiness at stall were of the thin-airfoil and combination thin-airfoil/trailing-edge stall categories. As indicated by the $C_{l,rms}$ data presented above, the unsteadiness was more pronounced for the latter stall type. For the pure thin-airfoil stall airfoils, the low-frequency unsteadiness was much more discernible in the lift spectra versus the wake hot film. For example, Fig. 8 compares hot-film and lift-balance spectra for the NACA 64A010 airfoil at $\alpha = 10°$, which corresponds to maximum lift. The low-frequency peak at approximately 4 Hz was discernible in both spectra, but the peak was much sharper in the lift spectrum. Unfortunately, the lift spectrum also contained the unwanted contributions from the model and balance resonances. Detailed frequency data were acquired for this and the other two thin-airfoil stall airfoils and the frequencies were converted to Strouhal numbers and plotted as a function of angle of attack (Fig. 9). The values of the Strouhal number were very low and they showed a generally increasing trend with angle of attack, as with the LRN airfoil.[9] The slopes shown on the plot were determined from simple linear regression.

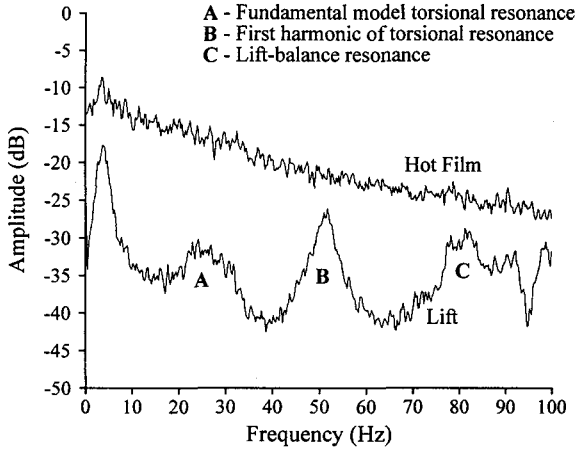

Fig. 8 Wake hot-film and lift spectra for the NACA 64A010 airfoil at $\alpha = 10°$. Spectra offset by 10 dB.

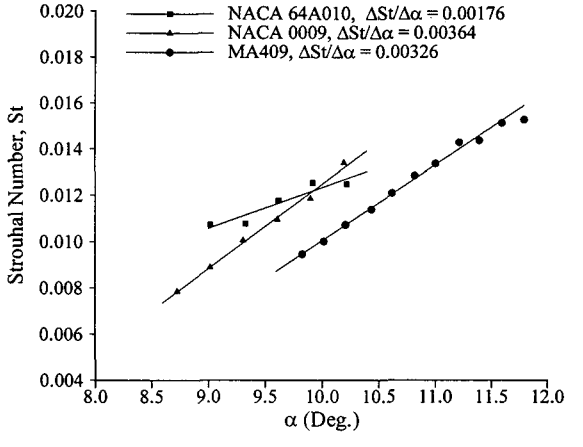

Fig. 9 Strouhal number variation with angle of attack for thin-airfoil stall airfoils. Frequency determined from the lift spectra.

It has already been noted above that the large-scale unsteadiness was most intense with the combination thin-airfoil/trailing-edge stall airfoils. Lift and hot-film power spectra for the LRN airfoil at α = 15° were already presented in Fig. 5. Note the intensity of the fundamental and its first harmonic which indicates the level of periodicity associated with the low-frequency oscillation. The variation in *St* with α for the three combination stall type airfoils is shown in Fig. 10. The results for the LRN airfoil were consistent with those presented by Bragg et al.[9] The data showed the same general trends as in Fig. 9, except that the Strouhal number showed a stronger dependence upon the angle of attack.

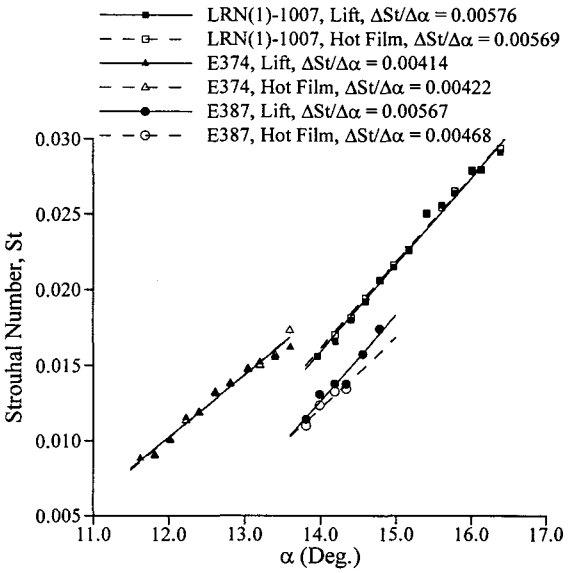

Fig. 10 Strouhal number variation with angle of attack for combination thin-airfoil/trailing-edge stall airfoils. Frequency source noted in legend.

Flow Visualization Results

The surface-oil-flow visualization method proved to be very valuable in defining the stall types of each of the airfoils since the boundary-layer characteristics were determined as the angle of attack was increased into stall. The boundary-layer features were very two-dimensional in character. This is in a time-averaged sense, since the oil is allowed to flow for 20 to 30 minutes. The two-dimensionality was characteristic of all airfoils tested, except for the E387, even for angles of attack above maximum lift. Figure 11 shows a boundary-layer state plot for the E374 airfoil. There was a separation bubble on the upper surface whose reattachment moved aft on the upper surface with increasing angle of attack, which is characteristic of the thin-airfoil stall type. There was also substantial turbulent boundary-layer separation which moved slightly forward on the upper surface with increasing angle of attack, which is characteristic of trailing-edge stall. Therefore, the E374 was classified as a having a combination of the two stall types. This flowfield behavior is also very similar to that of the LRN airfoil reported by Bragg et al.[9] and this comparison is further discussed below.

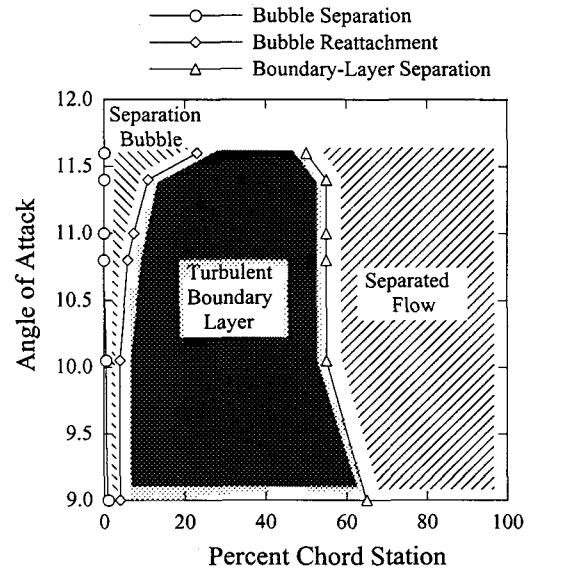

Fig. 11 E374 airfoil boundary-layer state versus angle of attack as determined from surface-oil-flow visualization.

Discussion

Airfoil Stall Type and Flowfield Unsteadiness

The data presented here show a distinct relationship between stall type and low-frequency/large-scale unsteady flow. Trailing-edge stall types exhibited minimal lift fluctuations until the angle of attack was increased well above $C_{l,max}$. Leading-edge stall types developed force fluctuations immediately past stall that accompanied the abrupt loss of lift. Thin-airfoil stall types exhibited larger fluctuations in lift which increased with angle of attack into stall and began to decrease beyond $C_{l,max}$. The most severe force fluctuations at stall were found on airfoils having a combination of thin-airfoil and trailing-edge stall. The fluctuations associated with the latter two stall types contained distinct low-frequency components. The data suggested that the low-frequency oscillation studied for the LRN airfoil also occurred on other airfoils with similar stalling characteristics.

Having formulated these conclusions based upon the present data, some comments can be made on previous investigations of two-dimensional airfoil stall. Beginning with the trailing-edge stall type, Jones[1] noted that "violent fluctuations" existed, but not until after maximum lift was obtained. In fact, judging from his observations he is likely referring to the bluff-body shedding regime. In this study, bluff-body shedding did not occur for trailing-edge stall airfoils until $\alpha >$ 20°. Essentially, he reports only "minor" fluctuations near maximum lift. This is consistent with McCullough and Gault[4] who do not report any unsteady characteristics for trailing-edge stall.

For airfoils having the leading-edge stall type, McCullough and Gault[4] note two different cases of unsteady flow. The stall of the NACA 63_1-012 was found to be so violent that, "the tunnel speed was reduced immediately after the occurrence of the stall." This observation is very consistent with the sharp increase in $C_{l,rms}$ just after $C_{l,max}$ was attained for the E472 airfoil in Fig. 7b. Gault[5] described the unsteady stalling behavior of an NACA 63-009 airfoil as involving a cyclic change between stalled and unstalled conditions at $C_{l,max}$ and that the flow was part of a circulatory motion above the airfoil surface. Although McCullough and Gault[4] classify this airfoil as having a leading-edge stall type, they describe the post-stall flow as more similar to thin-airfoil stall than leading-edge stall. Thus, the flowfield may contain weak low-frequency unsteadiness similar to the thin-airfoil stall airfoils in the present data. This is not unlikely, since a reduction in Reynolds number may cause the stall type of the NACA 63-009 to change to the thin-airfoil stall type.

The rise of lift fluctuations $C_{l,max}$ is a common characteristic of airfoils exhibiting the thin-airfoil stall. Even in the first investigations, Jones[1] noted the "violent force fluctuations" which were quasi-periodic near $C_{l,max}$, but quickly became irregular at lower or higher incidences. These observations are consistent with the very small angle of attack range for which a definite frequency was discernible in the present data (see Fig. 9). In their study of thin-airfoil stall on the NACA 64A006 airfoil, McCullough and Gault[6] reported "large [and] relatively low-frequency fluctuations of the velocity associated with the separated boundary layer" at $C_{l,max}$. In fact, they even estimated a frequency of the oscillation which corresponds to $St \approx 0.09$. This is much larger than those presented here, but also much smaller than the benchmark value of 0.20. Further, the authors noted that the (mean) lift data in the vicinity of stall showed considerable scatter which they attributed to the buffeting of the model. Again, this would suggest an increase in the fluctuating lift not unlike that shown in Fig. 7d. McCullough and Gault[4] also studied the stall of a 4.23% thick double-wedge airfoil which had a sharp leading-edge. A separation bubble was immediately formed whence the angle of attack was changed. Again, the authors reported the presence of a circulatory motion associated with the airfoil flowfield, indicating low-frequency unsteadiness. Few anomalies arise when previous data are reviewed in light of the present data.

Comments on the Magnitude of the Fluctuating Lift

In a review article on normal force fluctuations on airfoils, Mabey[2] analyzes data from various sources from airfoils having different stall types. He proposes a linear relationship between fluctuating normal force and the extent of trailing-edge, boundary-layer separation, based on data for two-dimensional airfoils at Reynolds numbers of 1.5-1.8 $\times$ 10^6 and Mach numbers from 0.5 to 0.9. He refers to the normalized separation length as the distance from the leading edge to the separation point per unit chord (x_{sep} /c). For airfoils with trailing-edge stall, this length decreases as the angle of attack is increased. Mabey proposes that, as the separation length decreases the magnitude of the force fluctuations increase linearly. An analysis of the present data for the trailing-edge stall type shows that a linear relationship may be too simplistic. The magnitudes of the $C_{l,rms}$ were higher and more strongly dependent upon the separation length in Mabey's data, than for the present data.

The present data are plotted in this way for the trailing-edge stall Ultra-Sport and the combination leading-edge/trailing-edge stall CLARK-Y along with Mabey's linear prediction (Fig. 12). The experimental $C_{l,rms}$ values fall well below this line. It is possible that the differences are attributable to the low-Reynolds number at which the present data were acquired. For example, Fig. 12 shows data for the NACA 63-018 section with aspect ratio 4, at Re = 500,000. There is much better agreement with the present data at Re = 300,000. Mabey notes that in even in the two-dimensional case for the NACA 63-018 (at Re = 500,000), the maximum normal force rms is 0.05, which compares very well with the present data. Therefore, the applicability of the Mabey's linear prediction may be limited to higher Reynolds and Mach numbers.

There are some caveats within these comparisons of fluctuating force data. Mabey provides no information about the bandwidth of the fluctuating normal force data. At the same time he comments on the effects of force-balance frequency response, but

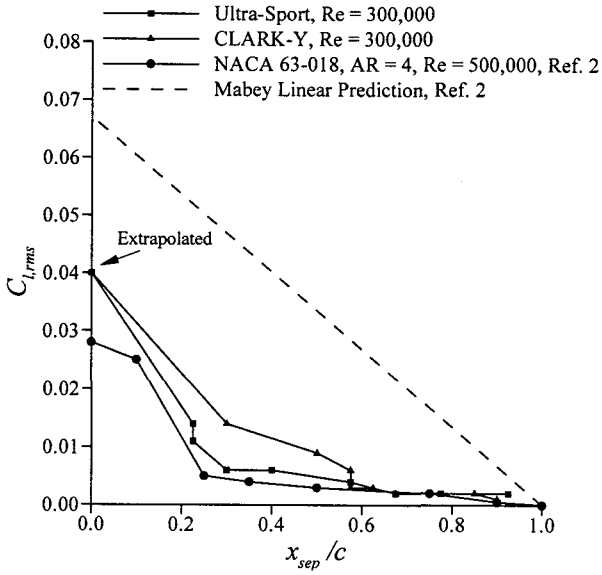

Fig. 12 Comparison of the variation in fluctuating lift versus distance from airfoil leading edge to boundary-layer separation point (x_{sep}/c).

does not quantify this in terms of fluctuating normal force. He also makes approximations about the extent of separation, which may not be exactly correct. In spite of these difficulties, the order of magnitude of the $C_{l,rms}$ data are comparable.

The Thin-airfoil Stall Type

The thin-airfoil stall type is of special interest in this study because of the large separation bubble which forms on the upper surface as the angle of attack is increased. The low-frequency unsteadiness associated with this type of stall was briefly discussed above, and is now presented in more detail as it relates to the leading-edge laminar separation bubble. The first evidence of a bubble on the NACA 64A010 airfoil is the reduction of the lift curve slope at $\alpha \approx 4°$ in Fig. 7d. It is likely that there was already a small bubble that has broken down into a long bubble, as described by Tani,[22] and this would also result in an attendant increase in drag. The boundary-layer state plot, derived from the flow visualization (Fig. 13) shows how rapidly this bubble grows as the angle of attack is increased. Also, note that the trailing-edge separation is minimal, thus resulting in the thin-airfoil designation. The bubble reattachment location in the oil-flow pattern at higher angles of attack was somewhat ambiguous (±5 % chord) and likely resulted from this region being very unsteady. This is not unexpected as Mabey[23] suggests that this region is the most unsteady part of the bubble, in terms of fluctuating pressure. The frequency data in Fig. 9 for these airfoils indicates that the unsteadiness occurs at very low frequencies. Mabey[2] shows fluctuating lift spectra for stalling airfoils which have frequency peaks that convert to Strouhal numbers of 0.011 (at $\alpha = 8.5°$) and 0.013 (at $\alpha = 10.0°$) which would fit nicely on the plot in Fig. 9. Unsteadiness in large separation bubbles is not uncommon and low-frequency disturbances have been documented for bubbles associated with a backward-facing step or blunt flat plate.[24,25] The low-frequency unsteadiness is of practical importance as Mabey[2] indicates that buffet at these low frequencies are more likely than higher frequencies to excite aircraft structural modes.

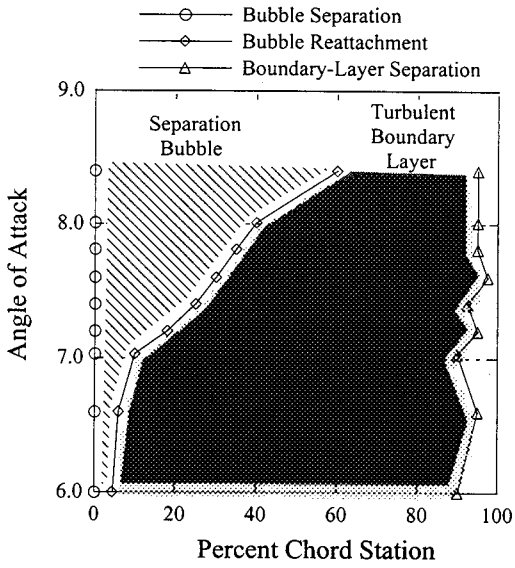

Fig. 13 NACA 64A010 airfoil boundary-layer state versus angle of attack as determined from surface-oil-flow visualization.

The Thin-airfoil and Trailing-edge Stall Combination

The fluctuating lift data presented here show an alarming trend for the combination thin-airfoil and trailing-edge stall cases. The maximum $C_{l,rms}$ associated with these airfoils is nearly double the maxima of the thin-airfoil stall types. Also, the low-frequency unsteadiness is very pronounced in both the lift and in the wake (see Fig. 10). From the data acquired in this study, it is apparent that this low-frequency oscillation studied in detail for the LRN airfoil occurs in much the same form for the other airfoils. A comparison of the time signals is shown in Fig. 14. All three time series show the extremely intense and low-frequency lift oscillation associated

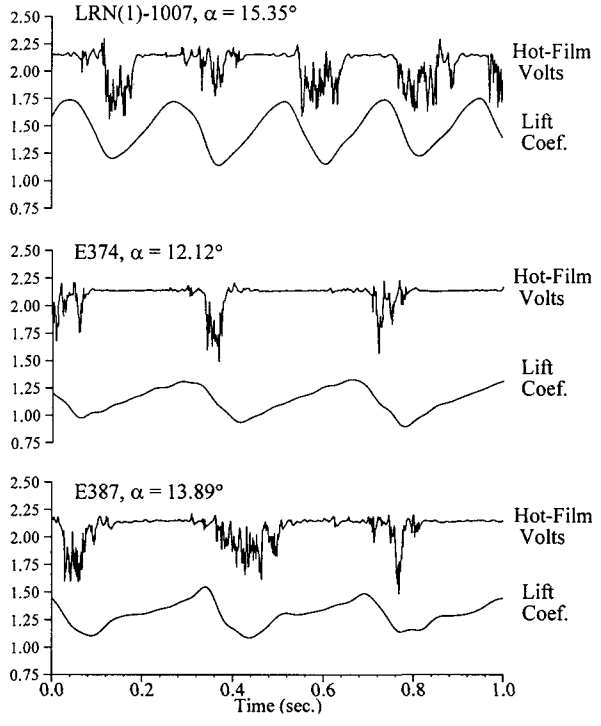

Fig. 14 Wake hot-film voltage and lift coefficient time series for the combination thin-airfoil/trailing-edge stall airfoils at angles of attack near maximum mean lift.

with the unsteadiness. The total fluctuation in C_l is about 37% of the mean for the LRN, about 35% of the mean for the E374 and about 30% of the mean for the E387. While the value of 37% for the LRN is lower than the 50% reported by Zaman et al.,[3] it is still very large. The wake hot-film voltage time series for both airfoils shows the periodic decrease in velocity as the airfoil stalls and the wake increases in size, causing the hot-film to be engulfed in low-speed fluid. As the flow reattaches and the wake decreases in size, the velocity voltage is higher and more uniform.[11] The time series data also show that the oscillation frequency is higher for the LRN(1)-1007 than for the E374 and E387. This is evident in the frequency data given in Fig. 10.

As previously discussed with thin-airfoil stall, the frequency is considered extremely low and may be related to the leading-edge bubble present on these airfoils (e.g., see Fig. 11) in the same way as for the thin-airfoil stall. The LDV flowfield measurements of Broeren and Bragg[10] performed on the LRN upper surface showed that the oscillation was related to the quasi-periodic growth and bursting of the leading-edge bubble. The "bursting of the bubble" occurred when the bubble reattachment merged with the trailing-edge separation. Not surprisingly, Mabey[2] describes a similar scenario of a downstream moving bubble reattachment merging with an upstream moving trailing-edge separation on a supercritical airfoil. This may explain why the lift fluctuations are more severe for the combination stall type case. That is, for pure thin-airfoil stall, the amount of trailing-edge separation is very small and the force fluctuations are smaller in magnitude. This suggests that the trailing-edge separation may amplify, or enhance, the unsteadiness in the separation bubble. However, more detailed measurements would be required to validate this theory.

A "superposition" type of analysis may be applied to summarize the entire data set. That is, Mabey[2] proposes that the movement of the trailing-edge separation contributes to some of the force fluctuations and that there may be separation bubble excitation which also contributes to the force fluctuations. Given the present data, it would seem that Mabey is correct in that airfoils with trailing-edge separations have low lift fluctuations at stall ($C_{l,rms} < 0.04$) and airfoils with large separation bubbles, like the thin-airfoil stall category, have moderate to high lift fluctuations at stall ($0.04 < C_{l,rms} < 0.08$). For airfoils having both large leading-edge bubbles and trailing-edge separations the lift fluctuations are indeed very high ($C_{l,rms} > 0.08$). This is a very simple analysis of a complex phenomenon. However, it may well provide the framework for determining the relative contributions of leading-edge and trailing-edge separations to force fluctuations on stalled airfoils.

Summary and Conclusions

Time-dependent lift measurements have been carried out on 12 airfoils with different stalling characteristics to determine the influence of stall type on low-frequency unsteadiness at stall. In addition to the lift data, wake hot-film data, frequency data and flow visualization data were acquired at a Reynolds number of 300,000. The lift force fluctuations were determined from the root-mean-square value of the fluctuating lift after low-pass filtering the data with a 20 Hz cut-off to remove unwanted contributions from model structural and lift-balance resonances.

The data presented in this paper show a distinct relationship between stall type and low-frequency/large-scale unsteady flow. Trailing-edge stall airfoils experience the least lift fluctuation at stall ($C_{l,rms} < 0.04$). For leading-edge stall airfoils the lift fluctuations increase sharply to $C_{l,rms} \approx 0.04$ with the abrupt loss of lift associated with this stall type. For thin-airfoil stall types, the fluctuating lift begins to

increase substantially in magnitude before the stall and has peak values of $C_{l,rms} < 0.08$, nearly double that of the previous two stall types. For these airfoils, distinct low-frequency oscillations, occurring at Strouhal numbers less than 0.02, are present in the fluctuating lift spectra. This behavior is likely related to unsteadiness in the large laminar separation bubble associated with this stall type. A combination of thin-airfoil and trailing-edge stall types results in $C_{l,rms}$ magnitudes which are nearly double that for pure thin-airfoil stall types. The energy is also contained within low-frequency oscillations detectable in the lift and wake hot-film spectra. The data suggest that the low-frequency oscillation studied for the LRN(1)-1007 airfoil also occurs on other airfoils with similar stalling characteristics. It appears that the unsteadiness associated with the laminar separation bubble is amplified by the trailing-edge separation, resulting in the large lift fluctuations. However, more research is necessary to completely validate this conclusion. Finally, the low-frequencies associated with the latter two cases are of practical importance since buffet at these frequencies may be likely to excite aircraft wing structural modes.

Acknowledgments

This work was funded through a NASA Graduate Student Researchers Program Fellowship. The authors wish to acknowledge K.B.M.Q. Zaman of the NASA Lewis Research Center for his contributions to this research.

References

1. Jones, B.M. "An Experimental Study of the Stalling of Wings," *Aeronautical Research Council Reports and Memoranda (ARC R&M)*, No. 1588, Dec. 1933.

2. Mabey, D.G., "Review of Normal Force Fluctuations on Aerofoils with Separated Flow," *Progress in Aerospace Sciences*,Vol. 29, 1992, pp. 43-80.

3. Zaman, K.B.M.Q., McKinzie, D.J., and Rumsey, C.L., "A Natural Low-Frequency Oscillation Over Airfoils Near Stalling Conditions," *Journal of Fluid Mechanics*, Vol. 202, 1989, pp. 403-442.

4. McCullough, G.B. and Gault, D.E., "Examples of Three Representative Types of Airfoil-Section Stall at Low-Speed," NACA TN 2502, Sept. 1951.

5. Gault, D.E., "Boundary-Layer and Stalling Characteristics of the NACA 63-009 Airfoil Section," NACA TN 1894, June 1949.

6. McCullough, G.B., and Gault, D.E., "Boundary-Layer and Stalling Characteristics of the NACA 64A006 Airfoil Section," NACA TN 1923, Aug. 1949.

7. Bragg, M.B., Heinrich, D.C., and Khodadoust, A., "Low-Frequency Flow Oscillation over Airfoils near Stall," *AIAA Journal*, Vol. 31, No. 7, July 1993, pp. 1341-1343.

8. Bragg, M.B., Heinrich, D.C., and Zaman, K.B.M.Q., "Flow Oscillation Over Airfoils Near Stall," ICAS Paper 94-4.5.2, 19th Congress of the International Council of the Aeronautical Sciences Conference Proceedings, Vol. 2, Sept. 1994, pp. 1639-1648.

9. Bragg, M.B., Heinrich, D.C., Balow, F.A., and Zaman, K.B.M.Q., "Flow Oscillation Over an Airfoil Near Stall," *AIAA Journal*, Vol. 34, No. 1, Jan. 1996, pp. 199-201.

10. Broeren, A.P., and Bragg, M.B., "Phase-Averaged LDV Flowfield Measurements About an Airfoil in Unsteady Stall," AIAA Paper 96-2494-CP, Proceedings of the 14th AIAA Applied Aerodynamics Meeting, New Orleans, June 1996, pp. 921-931.

11. Broeren, A.P., "Phase-Averaged Flowfield Measurements About an Airfoil in Unsteady Stall," M.S. Thesis, University of Illinois at Urbana-Champaign, 1996.

12. Farren, W.S. "The Reaction on a Wing Whose Angle of Incidence is Changing Rapidly— Wind-Tunnel Experiments with a Short-Period Recording Balance," *Aeronautical Research Council Reports and Memoranda (ARC R&M)*, No. 1648, Jan. 1935.

13. Reda, D.C., "Observations of Dynamic Stall Phenomena Using Liquid Crystal Coatings," *AIAA Journal*, Vol. 29, No. 2, Feb. 1991, pp. 308-310.

14. Bragg, M.B., Khodadoust, A., and Spring, S. A. "Measurements in a Leading-Edge Separation Bubble due to a Simulated Airfoil Ice Accretion," *AIAA Journal*, Vol. 30, No. 6, June 1992, pp. 1462-1467.

15. Selig, M.S., Guglielmo, J.J., Broeren, A.P., and Giguère, P., *Summary of Low-Speed Airfoil Data— Volume 1*, SoarTech, Virginia Beach, VA, 1995.

16. Selig, M.S., Lyon, C.A., Giguère, P., Ninham, C.P., and Guglielmo, J.J., *Summary of Low-Speed Airfoil Data—Volume 2*, SoarTech, Virginia Beach, VA, 1996.

17. Lyon, C.A., Broeren, A.P., Giguère, P., Gopalarathnam, A., and Selig, M.S., *Summary of Low-Speed Airfoil Data—Volume 3*, SoarTech, Virginia Beach, VA, 1997.

18. Giguère, P., and Selig, M.S., "Freestream Velocity Corrections for Two-Dimensional Testing with Splitter Plates," *AIAA Journal*, Vol. 35, No. 7, July 1997, pp. 1195-1200.

19. Coleman, H.W., and Steele, W.G., *Experimentation and Uncertainty Analysisfor Engineers*, John Wiley and Sons, New York, 1989.

20. McGee, R.J., Walker, B.S., and Millard, B.F., "Experimental Results for the Eppler 387 Airfoil at Low-Reynolds Numbers in the Langley Low-Turbulence Pressure Tunnel," NASA TM 4062, Oct. 1988.

21. Selig, M.S., Guglielmo, J.J., Broeren, A.P., and Giguère, P., "Experiments on Airfoils at Low-Reynolds Numbers," AIAA Paper 96-0062, Jan. 1996.

22. Tani, I., "Low-Speed Flows Involving Separation Bubbles," *Progress in Aeronautical Sciences*, Vol. 5, 1964, pp. 70-103.

23. Mabey, D.G., "Analysis and Correlation of Data on Pressure Fluctuations in Separated Flow," *Journal of Aircraft*, Vol. 9, No. 9, Sept. 1972, pp. 642-645.

24. Driver, D.M., Seegmiller, H.L., and Marvin, J.G., "Time-Dependent Behavior of a Reattaching Shear Layer," *AIAA Journal*, Vol. 25, No. 7, July 1987, pp. 914-919.

25. Kiya, M., and Sasaki, K., "Structure of a Turbulent Separation Bubble," *Journal of Fluid Mechanics*, Vol. 137, 1983, pp. 83-113.